Earth and Planetary Science Letters 452 (2016) 247–257

Contents lists available at ScienceDirect

Earth and Planetary Science Letters

www.elsevier.com/locate/epsl

Synchronicity of Kuroshio Current and climate system variability since the Last Glacial Maximum

Xufeng Zheng [a,*], Anchun Li [b], ShuhJi Kao [c], Xun Gong [d], Martin Frank [e], Gerhard Kuhn [d], Wenju Cai [f], Hong Yan [g], Shiming Wan [b], Honghai Zhang [h], Fuqing Jiang [b], Edmund Hathorne [d], Zhong Chen [a], Bangqi Hu [i]

[a] Key Laboratory of Marginal Sea Geology, South China Sea Institute of Oceanology, Chinese Academy of Sciences, Guangzhou, 510301, China
[b] Key Laboratory of Marine Geology and Environment, Institute of Oceanology, Chinese Academy of Sciences, 7 Nanhai Road, Qingdao, 266071, China
[c] State Key Laboratory of Marine Environmental Science, Xiamen University, Xiamen, China
[d] Alfred-Wegener-Institut, Helmholtz-Zentrum für Polar- und Meeresforschung, Am Alten Hafen 26, 27568, Bremerhaven, Germany
[e] GEOMAR Helmholtz Centre for Ocean Research Kiel, Kiel, Germany
[f] CSIRO Oceans and Atmosphere Flagship, Aspendale, Victoria 3195, Australia
[g] State Key Laboratory of Loess and Quaternary Geology, Institute of Earth Environment, Chinese Academy of Sciences, Xi'an, China
[h] Rosenstiel School of Marine and Atmospheric Science, University of Miami, Miami, FL, USA
[i] Key Laboratory of Marine Hydrocarbon Resources and Environmental Geology, Qingdao Institute of Marine Geology, Ministry of Land and Resources, Qingdao 266071, China

ARTICLE INFO

Article history:
Received 24 November 2015
Received in revised form 14 July 2016
Accepted 17 July 2016
Available online 4 August 2016
Editor: H. Stoll

Keywords:
Kuroshio Current
North Pacific subtropical gyre
ENSO
monsoon
precession

ABSTRACT

The Kuroshio Current (KC) is the northward branch of the North Pacific subtropical gyre (NPG) and exerts influence on the exchange of physical, chemical, and biological properties of downstream regions in the Pacific Ocean. Resolving long-term changes in the flow of the KC water masses is, therefore, crucial for advancing our understanding of the Pacific's role in global ocean and climate variability. Here, we reconstruct changes in KC dynamics over the past 20 ka based on grain-size spectra, clay mineral, and Sr–Nd isotope constraints of sediments from the northern Okinawa Trough. Combined with published sediment records surrounding the NPG, we suggest that the KC remained in the Okinawa Trough throughout the Last Glacial Maximum. Together with Earth-System-Model simulations, our results additionally indicate that KC intensified considerably during the early Holocene (EH). The synchronous establishment of the KC "water barrier" and the modern circulation pattern during the EH highstand shaped the sediment transport patterns. This is ascribed to the precession-induced increase in the occurrence of La Niña-like state and the strength of the East Asian summer monsoon. The synchronicity of the shifts in the intensity of the KC, Kuroshio extension, and El Niño/La Niña-Southern Oscillation (ENSO) variability may further indicate that the western branch of the NPG has been subject to basin-scale changes in wind stress curl over the North Pacific in response to low-latitude insolation. Superimposed on this long-term trend are high-amplitude, large century, and millennial-scale variations during last 5 ka, which are ascribed to the advent of modern ENSO when the equatorial oceans experienced stronger insolation during the boreal winter.

1. Introduction

The Kuroshio Current (KC), known as a strong western boundary current in the North Pacific Ocean, transports warm, highly saline waters from low to middle latitudes at relatively high speed (Hu et al., 2015). Variations in the KC's flow intensity and path have a substantial impact on the regional climate of East Asia (Hu et al., 2015), and characterize hydrographic and biogeochemical features in downstream regions, e.g., the East China Sea (ECS), south of Japan, and the East Sea (Sea of Japan) (Guo et al., 2012).

On seasonal and inter-annual scales, the intensity of the KC is affected by the East Asian monsoon and El Niño/La Niña-Southern Oscillation (ENSO) (Hu et al., 2015). These climate variations lead to basin-scale changes in surface winds over the North Pacific, which, in turn, modulate the southward transport of water mass in the inner ocean based on the Sverdrup theory (Eq. (1)) and the intensity of the northward flow of the KC at the western boundary (Hu et al., 2015). However, the teleconnection between KC dynam-

* Corresponding author.
E-mail address: zxf@scsio.ac.cn (X. Zheng).

http://dx.doi.org/10.1016/j.epsl.2016.07.028
0012-821X/

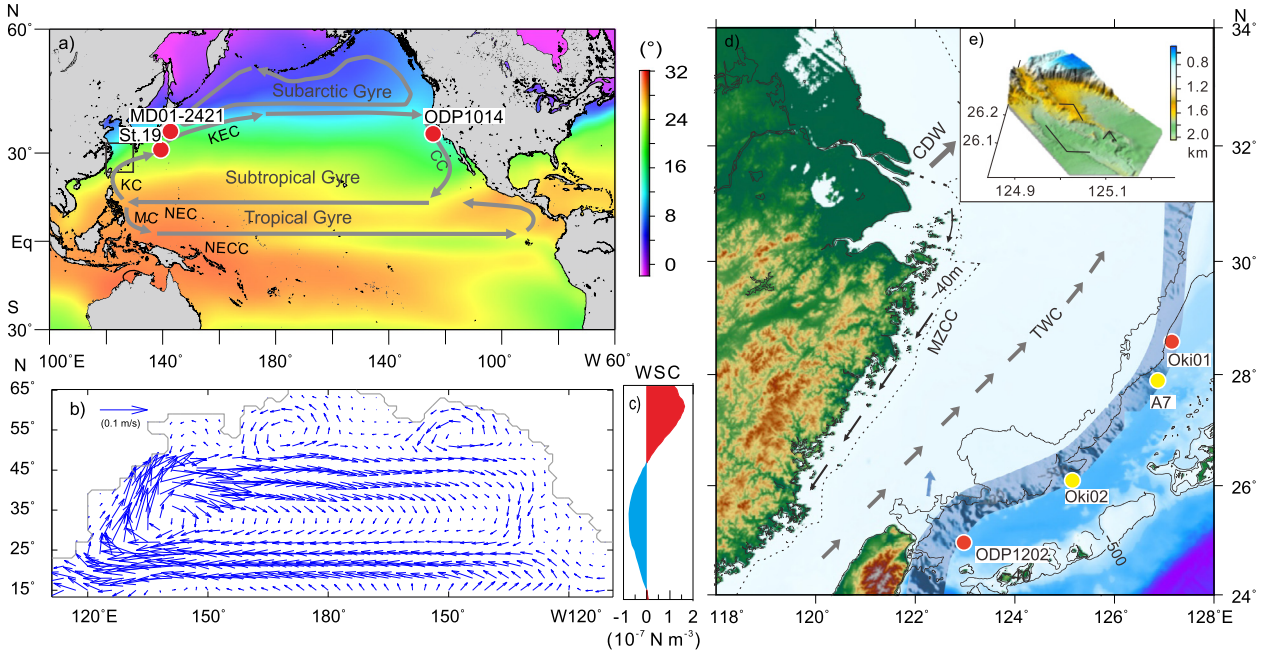

Fig. 1. The current system (small grey arrow lines) and sea surface temperature distribution of the Pacific Ocean during: a) La Niña (January, 1999). b) ocean currents (m/s) at 0∼300 m depth at the Late Holocene, as simulated in the COSMOS Model. c) Pacific zonally averaged wind stress curl at present (Hu et al., 2015). d) a schematic map, enlargement of the black square in a), for the topography and current system in the East China Sea (ECS), cores referred. **KC** = Kuroshio Current; **MZCC** = Min-Zhe Coastal Current; **TWC** = Taiwan Warm Current; **CDW** = Changjiang Diluted Water in summer. The dashed line represents −40 m isobath. The cores with yellow color were analyzed in this study. The red color is that referred. e) The Chiwei Island submarine canyon system from which core Oki02 was retrieved. (For interpretation of the references to color in this figure legend, the reader is referred to the web version of this article.)

ics and the millennial to orbital timescale tropical climate state, which have been proposed to have changed with the precession cycle (Clement et al., 1999; Schneider et al., 2014), remains elusive.

$$M_y = \frac{1}{\beta}(\nabla \times \tau)_k \quad (1)$$

The route of the KC exhibits meandering in the mid-latitude, central Pacific Ocean, especially to the south of Japan. As the meandering path of the KC can migrate spatially, a useful way to index the KC path has proven to be difficult. Although meandering is also observed along the density front of the KC in the Okinawa Trough, the main body of the KC is relatively stable due to topographic constraints (Andres et al., 2015). The high sedimentation rate, advantageous topography condition in the Okinawa Trough, and tight connection with low latitude climate make the Okinawa Trough an ideal location to reconstruct the history of the KC and its link to low latitude climate.

The present day KC enters the southern Okinawa Trough, flows along the outer shelf of the ECS, and exits through Tokara Strait (Fig. 1). However, a debate exists regarding the main pathway of the KC in the past. It has been argued that the KC was deflected to the east part of the Okinawa Trough during the Last Glacial Maximum (LGM) and has reentered the Okinawa Trough since around 7.1 ka (Dou et al., 2010; Jian et al., 2000). For instance, clay mineral and geochemical indices in the middle and northern Okinawa Trough revealed that the increased contribution of sediment from Taiwan Island between ∼8.4 and 14 ka is an indicator of the reentrance of the KC into the Okinawa Trough (Dou et al., 2010, 2012; Li et al., 2015). Studies based on similar methods have, however, suggested that the KC was present in the Okinawa Trough during the LGM lowstand, and intensified during the early Holocene (EH) (Chen et al., 2011; Wang et al., 2015; Zheng et al., 2011). An increase in the pollen of Podocarpus at the topmost part of core DGKS9602 reveals that the KC may have been reinforced in the Holocene (Zheng et al., 2011), agreeing with sedimentological studies (Wang et al., 2015). However, as these proxies are integrations of multiple transport mechanisms and may produce non-unique solutions, a relatively independent KC index is needed to resolve the aforementioned ambiguities.

In order to better examine the past variability of KC intensity and route, and the connections between the KC and low latitude climate systems since the LGM, sediment core A7 situated in the path of the KC, retrieved from the northern Okinawa Trough (Fig. 1), was subject of this study. Varimax Principal Component Analyses (V-PCA) was applied to the complex grain-size matrix to isolate independent grain-size components related to the KC. This method has also been applied to nearby core Oki02, and revealed the East Asian winter monsoon history during the Holocene (Zheng et al., 2014). Sr–Nd isotopic analyses were utilized to constrain the provenance of the KC grain-size spectrum and will verify our conclusions. For a more expanded view of the connections of the current system in this study (Fig. 1), we combined our data with those of core Oki02, two Ocean Drilling Program cores, and one Marion Dufresne core from the high latitude North Pacific to elucidate the relationships between the middle latitude KC and low latitude Pacific climate systems. Moreover, we also reanalyzed the Earth-System-Model simulations for the LGM, 9 ka (a representative for the Early Holocene), and Pre-industrial condition (a representative for the Late Holocene) to assist in understanding the proxy-indicated LGM to Holocene anomalies in the KC.

2. Study area

The climate and oceanography in the Okinawa Trough is significantly influenced by the KC and the East Asian monsoon (Lee and Chao, 2003). Moreover, the KC is the most striking feature of the Okinawa Trough hydrography and constitutes a link between low- and mid-latitudes (Hu et al., 2015). Mooring and float observations revealed that the KC penetrates to greater depths as it progresses downstream. Specifically, it extends to the seafloor at the 1200 m isobath in the middle of the Okinawa Trough at the PN line (0.7 m/s), and is found even deeper at the 1500 to 2000 m isobaths south of Japan (Andres et al., 2015).

The KC exhibits temporal variability at scales ranging from seasonal variations in Kuroshio intrusions onto the shelf, to interannual transport variability, to multiyear meandering of the flow path south of Japan (Andres et al., 2015). Further downstream, the KC flows from northeastern Taiwan to southeastern Japan, where the current finally transits from a western boundary current into the Kuroshio extension, a vigorously meandering free jet.

According to the Sverdrup balance (Eq. (1)), the northward mass transport of wind-driven currents is equal to the curl of the wind stress (Sverdrup, 1947). The trade winds blow westwards in the tropics, and the westerlies blow eastward at mid-latitudes. This exerts a pressure on the subtropical ocean surface with a negative curl in the subtropical Pacific that results in an equatorward Sverdrup transport and an intense, narrow poleward current along the western boundary of the Pacific Ocean Basin (Fig. 1b, c) (Stommel, 1948).

The KC exhibits strong seasonal and interannual variability since it is situated in a geographical location where dynamic processes are controlled by the East Asian monsoon and ENSO (Hu et al., 2015). On a seasonal scale, summer southeastern monsoon winds produce a negative wind stress curl over the tropical Pacific, leading to an enhanced equatorward transport of water masses over the inner ocean of the NPG, and consequently an intensified northward transport of the KC at the western boundary (mass conservation) (Hu et al., 2015). The opposite situation occurs for the winter monsoon. Moreover, the alternating monsoonal winds mainly determine the water volume entering the South China Sea and that flowing northward into the Okinawa Trough (Qu et al., 2004). Meanwhile, seasonal switches of the East Asian monsoon can alter the KC intrusion onto the shelf, and thus the sediment transport pattern. An important feature is the KC "water barrier", which is referred to a section of the water column with an extremely low concentration of suspended material (<0.5 mg/dm^3) resulting from the intrusion of the subsurface-intermediate water of the KC. It stretches across the ECS continental shelf and obstructs the suspended matter from the shelf into the deep trough (Yang et al., 1992). The KC "water barrier" prevails during summer, and weakens during winter when the East Asian winter monsoon strengthens, resulting in a different sediment transport pattern, i.e., summer storage and winter export of sediments on the ECS shelf. Interannually, the intensity of the KC is closely related to ENSO events. During El Niño years, positive wind stress curl anomalies develop north of the equator, weakening the poleward transport of the KC; whereas, during La Niña years, the situation is reversed (Hu et al., 2015).

3. Materials and methods

3.1. Materials and age model

New data were acquired from piston core, A7 (126.98°E, 27.82°N, water depth 1264 m, and core length 4.5 m) that was recovered by R/V Kexue No. 1 during a cruise in 2001. The A7 coring site is located on the western slope of the northern Okinawa Trough (Fig. 1), ideal for trapping the offshore transport of suspended sediments from the ECS continental shelf (Zheng et al., 2014). Sediment in core A7 mainly consists of gray silty clay, with an ash layer at 1.02 to 1.10 m depth and several turbidity layers at 1.10 to 1.20 m depth (Fig. 2) (Sun et al., 2005). The sediment core was sectioned into 2-cm intervals after the cruise. The age model of A7 has been constructed based on 15 Accelerator Mass Spectrometry (AMS) ^{14}C datings of planktonic foraminifera (Fig. 2). Since a consistent constraint on the age model is critical for a later discussion of basin-wide synchronicity, and most of the cores referred in the western Pacific were calibrated to calendar age with a 400-yr reservoir age, we reconverted all AMS ^{14}C ages of core A7 and a nearby core Oki02 in the Okinawa Trough to calendar

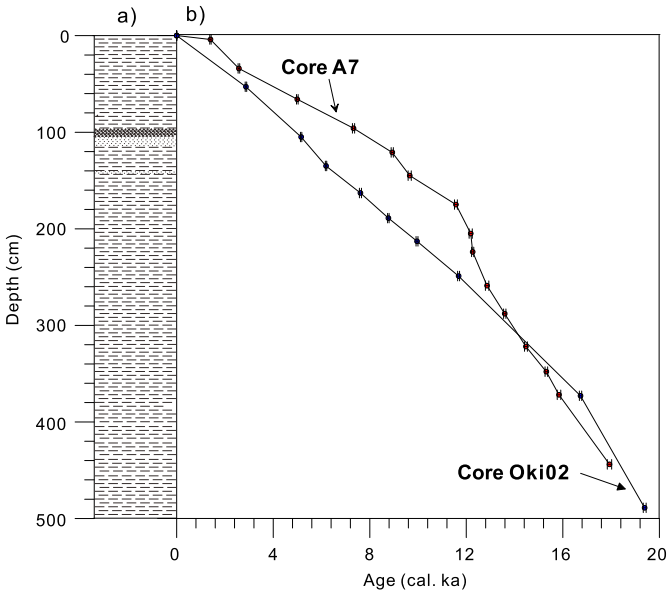

Fig. 2. Lithology for core A7, and age model for core A7 and Oki02. a) Log of lithologic changes against depth for core A7, with dashed lines representing laminations, black point layers referring to turbidity layers, and triangular symbols referring to volcanic ash. b) Age model of core A7 (red point) and Oki02 (blue point). (For interpretation of the references to color in this figure legend, the reader is referred to the web version of this article.)

years using the Calib 7.0 program via the latest calibration curve (i.e., MARINE13) with a 400-yr surface ocean reservoir correction and a Delta R-value of 58 ± 58 (http://calib.qub.ac.uk/marine/). We also included the K-Ah ash layer at 7165∼7303 cal yr BP as a time marker (Smith et al., 2013) (Fig. 2). The results show that the main transition points of core A7 are in line with those of core Oki02 and other cores in the Okinawa Trough (Diekmann et al., 2008; Kao et al., 2005; Zheng et al., 2014). This consistency suggests that the 400-yr reservoir age used in this study is reliable for the discussion below. Linear interpolation between dated layers in core Oki02 presents a 7.3 ka age for the K-Ah ash layer, which is in line with the 7.3 ka age estimated from lake sediments in Japan (Smith et al., 2013).

3.2. Methods

Grain size and clay mineral analyses were performed for core A7 according to Zheng et al. (2014). V-PCA analyses were applied to the time series grain-size spectrum of core A7 to elucidate mechanisms that are related to the KC pathway and intensity.

Surface features of sediment grains of several coarse layers in core A7 (38∼40, 58∼60, 110∼112, and 116∼118 cm) and core Oki02 (48∼50, 82∼84, and 156∼158 cm) were analyzed using a JEOL JXA-8100 electron probe micro-analyzer (EPMA). The Energy Dispersive Spectrometer (EDS) system affiliated with EPMA was adopted to detect the geochemical compositions of sediment grains. Samples for EPMA and EDS analyses were prepared according to an accepted pretreatment method of grain-size analyses (Zheng et al., 2014).

The radiogenic isotope composition of neodymium (Nd) and strontium (Sr) was measured on the siliciclastic fraction (AF2/OF3, see below) and suspended sediments from Taiwan rivers (Table S1). We used a leaching procedure following the method of Jiang et al. (2013). The AF2/OF3 (5∼18 μm) was extracted from bulk sediment based on Stokes' settling velocity principle (Fig. S1). Approximately 0.05 g dry sediment was totally dissolved using a mixture of concentrated HCl, HNO_3, and HF on a hot plate. Standard column-chromatography procedures were applied

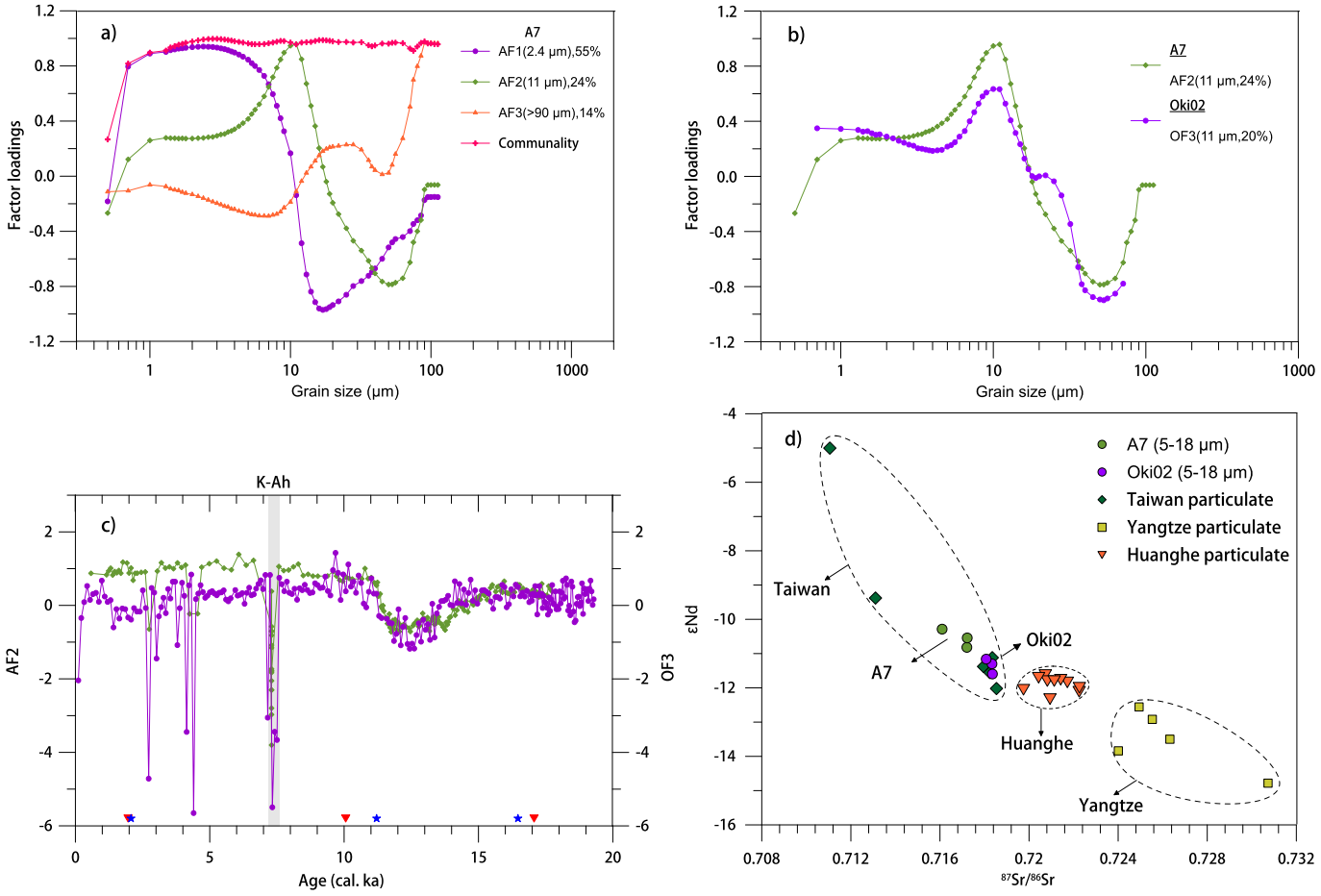

Fig. 3. a) Results of V-PCA analyses on the grain-size matrix of core A7. b) Grain-size spectrum of the KC (AF2: green, OF3: violet) for core A7 and Oki02, respectively. c) Secular variation of AF2 (green) and OF3 (violet), red stark, inverse triangle representing the depths for the extracted AF2 and OF3 grain-size fraction for Sr–Nd isotopic analyses, respectively. d) Sr and Nd radioisotope signature for AF2 and OF3 (Table S1), as compared to the present day suspended material collected in the Yangtze River (Luo et al., 2012), Huanghe River (Hu et al., unpublished), and rivers in Taiwan Island (Table S1). For consistency, we chose samples with a grain-size distribution similar to AF2 and OF3. (For interpretation of the references to color in this figure legend, the reader is referred to the web version of this article.)

to separate and purify Nd and Sr (Jiang et al., 2013). The Nd and Sr isotope compositions were measured on a Nu Instruments multi-collector inductively-coupled plasma mass spectrometer at the GEOMAR, Kiel, using ratios of 0.7219 for $^{146}Nd/^{144}Nd$ and 0.1194 for $^{88}Sr/^{86}Sr$ to correct for instrumental mass bias. All isotope results were normalized to the accepted values of the JNdi standard for Nd (0.512115) and of the NBS SRM 987 standard for Sr (0.710245) to account for instrument-specific offsets. The Nd isotope ratio was reported as εNd, which was the corrected $^{143}Nd/^{144}Nd = 0.512638$ (Jiang et al., 2013) and multiplied by 10000. External reproducibility was first estimated by repeated measurement of the in-house SPEX standard for Nd and the AA standard for Sr, and the isotope ratios were reported with 2σ uncertainties of ± 0.4 εNd units for Nd and ± 0.000024 for Sr.

Additionally, we also re-analyzed model simulations for the PI, i.e., LH (Wei and Lohmann, 2012), 9 ka, i.e., EH (Wei and Lohmann, 2012), and LGM (Gong et al., 2015) conditions. The model employed the Community Earth System Models (COSMOS), with the ocean of a formal horizontal resolution of $\sim 3^\circ \times 1.8^\circ$ and uneven 40 vertical layers, and the atmosphere of a horizontal resolution of $\sim 3.75^\circ \times 3.75^\circ$ and 19 vertical levels. The set-up details of these three numerical experiments were explained in Gong et al. (2015). In the model, KC strength refers to the northward velocity by the North Pacific western boundary current of 110∼140°E and 0∼300 m across 27°N and 34°N. The same method has been applied to analyze the paleo Gulf Stream heterogeneity (Gong et al., 2015).

Wavelet analyses were applied to analyze factor score of OF3 (see below), a proxy for paleo KC strength, to infer the teleconnection between the climate and current system. Prior to the analyses, OF3 was resampled at 20-yr intervals and filtered to reduce noise.

4. Results

4.1. V-PCA analyses on grain-size matrix

Fig. 3 shows the results of the V-PCA analyses on the grain-size matrix for core A7. Three principal grain-size components (AF1: 55%, AF2: 24%, and AF3: 14%), that account for 93% of the variance, were identified for core A7. The first mode (AF1) has a broad positive peak at 2.4 μm and a negative peak at 17 μm (Fig. 3). The second mode (AF2) has a peak at 11 μm and a trough around 50 μm (Fig. 3). The third mode (AF3) has a positive peak at 90 μm (Fig. 3). Four components (F1: 33%, F2: 33%, F3: 20%, and F4: 9%), that contribute to 95% of the variance for core Oki02, have been previously reported (Zheng et al., 2014). In this paper, we have renamed them OF1, OF2, OF3, and OF4 for symbol distinction (Fig. S1).

4.2. Sr–Nd isotope results

Sr and Nd isotope data for the samples of our study are displayed as $^{87}Sr/^{86}Sr$ versus εNd in Fig. 3d and Table S1. The

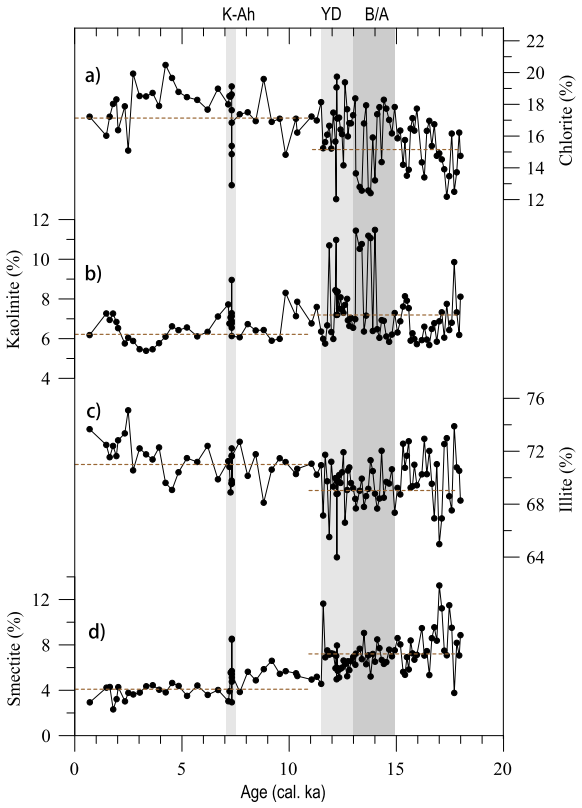

Fig. 4. Secular variations of clay mineral assemblages, including: a) smectite; b) illite; c) kaolinite; and d) chlorite for core A7.

$^{87}Sr/^{86}Sr$ ratios of AF2 and OF3 varied between 0.7161 and 0.7184, and εNd ratios ranged from −11.6 to −10.3. The $^{87}Sr/^{86}Sr$ ratios of suspended sediment from rivers in Taiwan Island ranged from 0.7111 to 0.7185, and εNd values varied between −12 and −5.

4.3. Mineral analyses

The proportional distribution profiles of the four major clay minerals of core A7 are shown in Fig. 4. The clay minerals were composed mainly of illite (64.0 to 75.1%), chlorite (12.0 to 20.5%), smectite (2.3 to 13.2%), and kaolinite (5.4 to 11.5%) (Figs. 4, 5). Smectite abundance peaked around 12% between 19.2 and 16 ka, and remained relatively high at 7% during the period between 16 and 12 ka. Starting in the EH, however, it decreased toward 4% and then became stable. The trend of kaolinite closely resembled that of smectite, apart from a relatively high value occurring between 13 and 14 ka. There was a generally increasing trend of the abundance of illite towards the Holocene. From 19.2 to 16 ka, illite showed a minimum of 66% and remained at 68% between 16 to 12 ka. Afterwards, the abundance increased abruptly to 72%. The percentage of chlorite was generally inversely-related with kaolinite. Moreover, it was more variable during 5∼2.5 ka than kaolinite.

Sediment grains of 48∼50 and 82∼84 cm in core Oki02 consisted mainly of K-feldspar, Na-feldspar, and quartz (Fig. S2). Likewise, sediment grains of 38∼40 and 58∼60 cm in core A7 were composed mainly of K-feldspar and quartz (Fig. S2). Sediment fractions of 156∼158 cm in core Oki02 contained mainly quartz and tephra (Fig. S2). However, sediment fractions of 110∼112 and 116∼118 cm in core A7 consisted mainly of tephra. Elongated vesicles, as well as fluidal textures, were observed in the structure of tephra, implying an origin from volcanic ashes (Fig. S3).

4.4. Modeling results

Our modeling results showed that the North Pacific western boundary current at 27°N was stronger during EH and late Holocene (LH) compared to the LGM conditions, with the largest value at the EH (Figs. 6 and 7). Our calculation of the North Pacific western boundary current has integrated the northward velocity between 110 and 140°E, fully covering the pathway uncertainties between the LGM and Holocene conditions. As shown in Fig. 7, the same sequence in the velocities of the North Pacific western boundary current was found at 34°N.

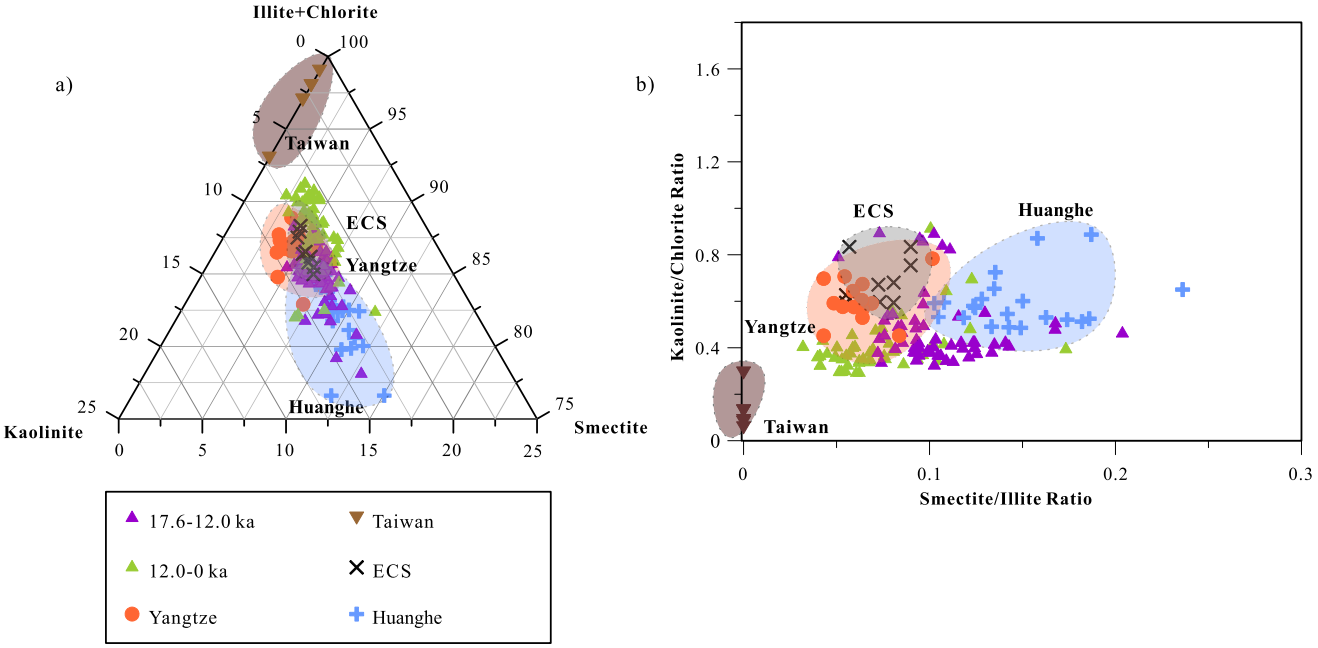

Fig. 5. End member analyses of provenance using: a) a ternary diagram of smectite-kaolinite-(illite + chlorite). b) Smectite/illite versus kaolinite/chlorite ratios. The green triangles represent an interval of 12.0 to 0 ka for core A7; the violet triangles show 17.6 to 12.0 ka for core A7; and the brown inverted triangles represent Taiwan rivers samples. The black crosses denote ECS Continental Shelf samples; the orange circles are the Yangtze River samples; and the blue crosses are the Huanghe River samples based on Zheng et al. (2014). (For interpretation of the references to color in this figure legend, the reader is referred to the web version of this article.)

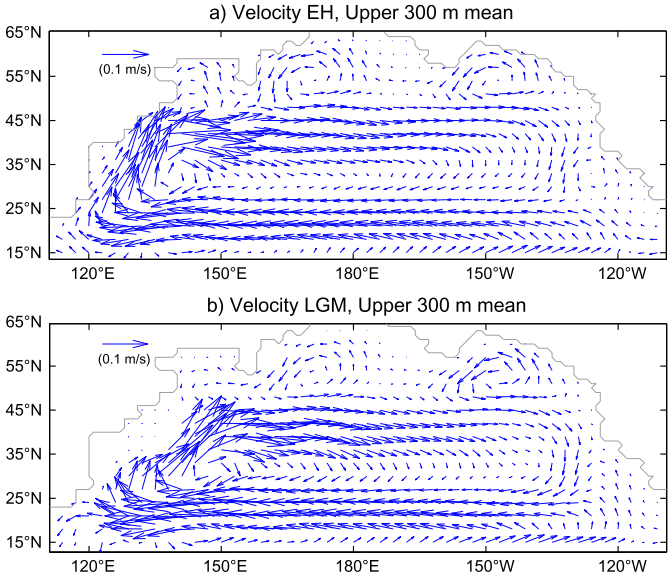

Fig. 6. Ocean currents (m/s) at 0∼300 m depth in the North Pacific Ocean, as simulated in the COSMOS Model during: a) EH; and b) LGM.

5. Discussion

5.1. Dynamic KC spectrum

Terrigenous particles deposited in marine sediments originated from distinct sources and underwent different modes of transport, which were characterized by specific grain-size distributions (Weltje and Prins, 2003). The grain-size distribution of the siliciclastic sediment fraction of core A7 consisted of three statistically relevant dynamic populations by Varimax Principal Component Analyses (Fig. 3). On the basis of the regional distribution of endmembers retrieved from suspended sediments in the Taiwan rivers, bottom nepheloid layers, and surface sediments of the ECS continental shelf, the three endmembers of core A7 were interpreted as KC silt (AF2), turbidity sand (AF3), and bottom nepheloid clay (AF1) related to winter monsoon intensity (see Supplementary Information) (Fig. 3a). The grain-size spectrum and long-term variation of AF2 agreed with OF3, a KC dynamic population previously reconstructed from nearby core Oki02 (Zheng et al., 2014) (Fig. 3). The grain-size spectra of core Oki02, i.e., OF1, OF2, OF3, and OF4, represented the winter monsoon-induced upper layer (UL) transport, the bottom nepheloid layer (BNL), the KC, and aeolian contributions, respectively (Zheng et al., 2014). In order to further assess the provenance of AF2/OF3, we separated the 5∼18 μm fraction from bulk sediment and measured its radiogenic Nd and Sr isotope composition (Fig. 3, Table S1). Suspended sediments collected from the Yangtze, Huanghe River, and rivers of Taiwan Island were used for comparison (Fig. 3, Table S1). We chose suspended sediment with a grain-size distribution (5∼20 μm) similar to AF2/OF3 (Fig. S1). The $^{87}Sr/^{86}Sr$ versus εNd plot clearly showed that the AF2/OF3 component originated from rivers of Taiwan Island. This suggested that AF2/OF3 was transported by KC to the Okinawa Trough. Therefore, the radiogenic isotope signature of AF2/OF3 supported the interpretation that AF2/OF3 represented KC dynamics (Fig. 3, Table S1). Overall, the temporal variation of AF2 and OF3 was consistent with various other KC proxies retrieved from the KC pathway from northeastern Taiwan to the coast of Japan (Fig. 8). Moreover, our modeling simulations presented the same

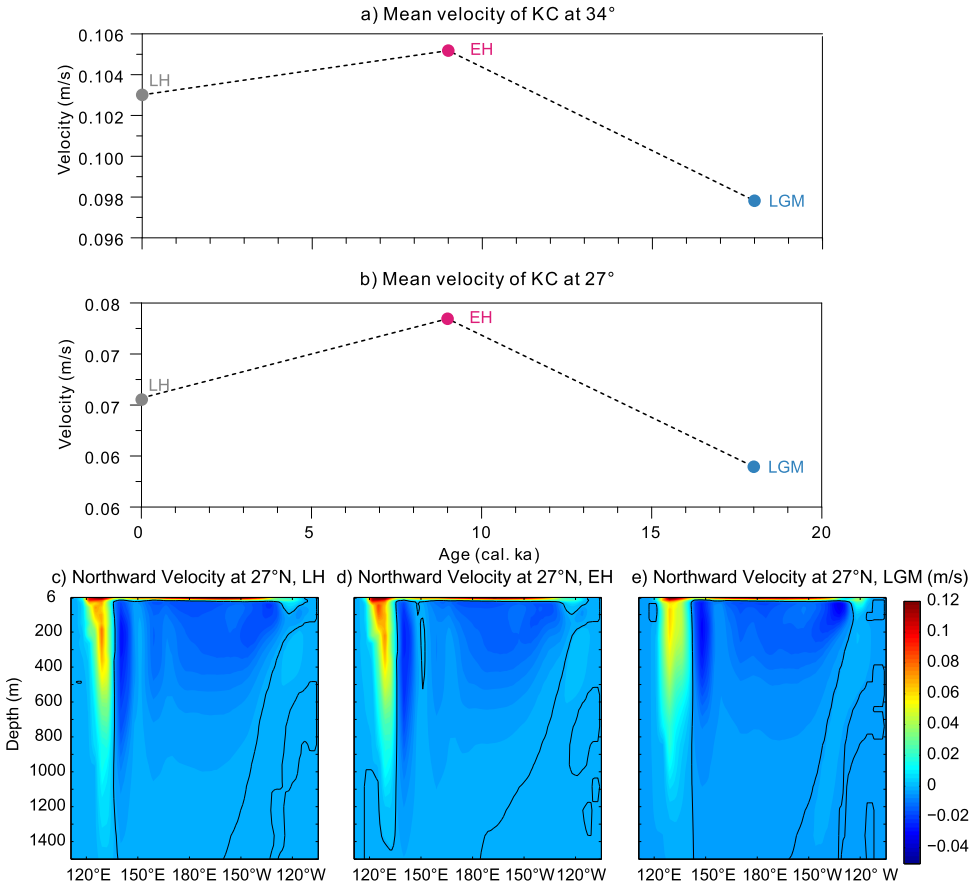

Fig. 7. Current velocity for KC at: a) 27°N and b) 34° during LH, EH, and LGM. Northward velocity profile for KC during: c) LH, d) EH, and e) LGM at 27°N, as simulated in the COSMOS Model.

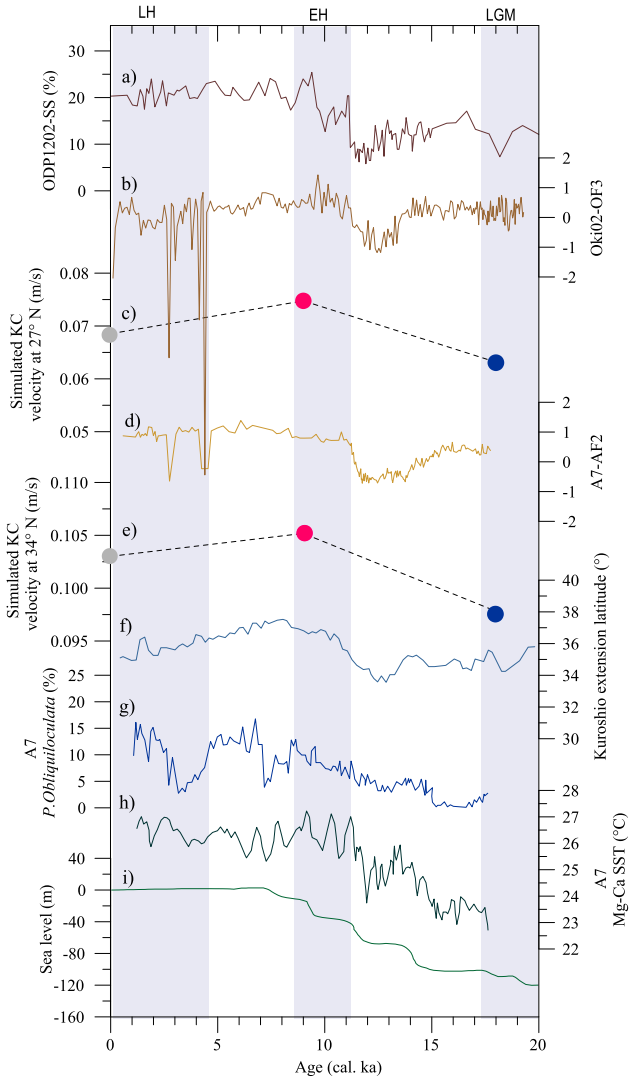

Fig. 8. a) Temporal variations of the percentage of the sortable silt (SS) fraction of core ODP1202 (Diekmann et al., 2008). b) The factor score of the KC index for AF2. c) KC strength at 27°N, as simulated in the COSMOS Model for LH, EH, and LGM. d) The factor score of the KC index for OF3. e) KC strength at 34°N, as simulated in the COSMOS Model for LH, EH, and LGM. f) Latitudinal variation of the Kuroshio extension, as revealed by the SST contrast between core St.19 and MD01-2421 (Yamamoto, 2009). g) *P. Obliquiloculata* abundance of core A7 (Xiang et al., 2007). h) Mg-Ca SST of core A7 (Sun et al., 2005). i) Sea level pattern in the western Pacific since the LGM (Liu et al., 2004).

sequences of KC changes among LH, EH and LGM, supporting our KC reconstructions at the A7 and Oki02 core sites (Fig. 8).

5.2. KC "water barrier" effects and provenance response since the early Holocene

As the most important current in the ECS, the KC exerts considerable influence on sediment transport patterns. The newly formed modern current system and the synchronous emergence of the KC "water barrier" during the EH altered the regional environment of the ECS considerably. Previous studies based on the sedimentology, paleontology, and biogeochemistry of sediment cores, indicated that the paleoenvironment of the Okinawa Trough and sediment provenance have changed since the EH (Diekmann et al., 2008; Dou et al., 2010, 2012; Kao et al., 2005; Oguri et al., 2000; Ujiié et al., 2001). The increased contribution of terrigenous sediments from Taiwan by the re-entrance and intensification of the KC has been proposed to account for the change in Nd isotope, rare earth elements, and clay mineral compositions since approximately 12 ka (Dou et al., 2010, 2012). The rise in sea level and the coastline retreat since the EH have also been proposed as leading causes of the change in terrigenous material proxy, i.e., $\delta^{13}C$, C/N ratio, and lignin phenol, and thus the sediment provenance transition appearing in the Okinawa Trough (Ujiié et al., 2001). However, our results provide a novel explanation for this development. The clay mineral assemblages showed a marked change since the EH (Fig. 4). The sediment source changed from main contributions of the Yangtze and Huanghe rivers to a mixture of the Yangtze River and shelf areas, with less contributions from Taiwan (Figs. 4 and 5). This is consistent with previous clay mineral studies on Oki02 and Oki01 cores (Zheng et al., 2014, 2015), supporting a basin-wide forcing, i.e., the KC "water barrier" accounting for this change. According to Diekmann et al. (2008), the increase of sortable silt (SS) content and the transition of clay mineral compositions in core ODP1202 in the southern Okinawa Trough since the EH was a response to the intensification of the KC. This is consistent with the cores in the middle and northern Okinawa Trough, and also the KC changes in our modeling simulations (Figs. 6 and 7), and thus supports the so-called "water barrier" theory (Zheng et al., 2014, 2015). We also observed that clay minerals exhibited fluctuations from LGM to deglacial period. This indicated that source regions of the clay minerals changed at a shorter time-scale due to a change of fluvial discharge of the Yangtze and Huanghe Rivers (Wang et al., 2015). However, the general trend of sediment provenance was less changed until the EH, when the KC was intensified and the KC "water barrier" was formed.

5.3. Fluctuation of the KC since the LGM

As previously mentioned, AF2 and OF3 represent indices for the grain sizes that are transported by, and sensitive to, the presence and strength of the KC, which has fluctuated since the LGM. Their overall temporal variability resembled the SS content of core ODP1202 and the ΔSST_{NWP} (Fig. 8). The SS of core ODP1202 was utilized to represent the variation in the KC dynamics. Large SS percentage in core ODP1202 suggests a strong current, and vice versa. The ΔSST_{NWP} represents the sea surface contrast between core St.19 and MD01-2421 in the western Pacific Ocean and was used to reflect the latitudinal variation of the Kuroshio extension (Yamamoto, 2009). Large ΔSST_{NWP} represents the northward migration of Kuroshio extension, vice versa. The AF2 and OF3 values exhibited relative stability from 19 to 14 ka, followed by a gradual weakening (Fig. 8). The equilibrium run also revealed a low current intensity and shallower penetration of the KC during the LGM (Figs. 6 and 7). However, the *P. obliquiloculata* abundance of core A7 reached a minimum, or even became extinct, during this interval (Xiang et al., 2007). The low *P. obliquiloculata* abundance could be associated with a low surface sea temperature and the invasion of coastal waters due to large seaward migration of the coastline, corroborated by the minimal Mg–Ca SST in core A7 (Liu et al., 2004; Sun et al., 2005). The AF2 and OF3 values decreased gradually beginning at 14 ka and reached a minimum at 12 ka, despite the stable sea level (Liu et al., 2004). This decline was concurrent with a decrease in SS content in cores ODP1202, as well as a reduction in Mg–Ca SST at A7 (Fig. 8). In addition, the *P. obliquiloculata* abundance exhibited a declining trend at A7 (Xiang et al., 2007). A southward migration of the Kuroshio extension also occurred at 12 ka (Yamamoto, 2009). Beginning in the EH, there was a considerable increase in AF2 and OF3, which peaked and attained a stable value at 10 ka, as well as the SS content in core ODP1202 (Fig. 8). Moreover, the *P. obliquiloculata* abundance and the Mg–Ca SST increased substantially in A7 (Sun et al., 2005). The intensified KC and the synchronous emergence of the KC "water barrier"

dramatically changed the regional environment of the ECS (Figs. 4 and 5).

The AF2 and OF3 values decreased abruptly between 7.3 and 7.1 ka. This transition is related to the turbidity layers occurring during 7.3 to 7.1 ka. The occurrence of volcanic tephra in the turbidity layers and the interbedding of volcanic tephra with turbidity layers revealed from EPMA-EDS analyses and detailed core description records (Fig. S3) may further imply that this change was possibly caused by the volcanic event. Based on the amplitude of the AF2 and OF3, large century-scale variations in the KC are inferred beginning at 5 ka, and were especially prominent from 4.2 to 2.7 ka (Fig. 8). EPMA-EDS analyses of these layers of the two cores demonstrated that they are mainly composed of terrigenous material, i.e., feldspar and quartz with less contribution of volcanic ash (Fig. S3), thus precluding the possibility of an influence of volcanic events. This interval coincided with the *Pulleniatina* Minimum Event (PME), which has been widely identified from the western Pacific to the Okinawa Trough (Lin et al., 2006; Xiang et al., 2007). A southward shift of the Kuroshio extension was also apparent (Yamamoto, 2009). In agreement with these proxy evidences, our modeling simulations also suggested a slowdown of the KC during the LH compared with the EH conditions, at both 27° and 34°N (Figs. 6 and 7).

5.4. Coherent variation of the KC and climate system since the LGM

The KC variability exhibited a long-term trend overprinted by short-term fluctuations (Fig. 9). The long-term trend appears to be coherent with precessional variability (Fig. 9). Since 12 ka, larger contributions of fine silt particles that characterize the KC grain-size end member (AF2 and OF3) corresponded to the main change of precessional forcing (Fig. 9).

As the northward branch of the NPG, the KC was closely correlated with the low latitude climate system, e.g., the ENSO and the East Asian monsoon, which in turn affected the basin-scale changes in surface winds over the North Pacific (Hu et al., 2015; Qu et al., 2004). The main linkage of the KC variability and ENSO dynamics was the clock-wise flow of the NPG. Modeling, using the Zebiak–Cane coupled ocean-atmosphere model, revealed that seasonal variations in insolation dominated by the precession cycle had a significant effect on tropical climate, i.e., ENSO variability, through an "ocean dynamical thermostat" mechanism on glacial-interglacial time scales (Clement et al., 1999, 2000). The hypothesized mechanism has been related to the Earth passing through the perihelion at the beginning of the calendar year at present (Clement et al., 1999). In the boreal late summer–early autumn of the EH, when the equatorial oceans received less heat during boreal winter, the ENSO power reached a minimum at 9 ka (Fig. 9) (Clement et al., 1999). The dampened ENSO variation during the early to middle Holocene climate optimum corresponded to La Niña-like tropical Pacific, where the climatology was suggested to be a result of similar physics operating on a variety of time scales (Clement et al., 2000). Therefore, the easterly wind anomalies in the tropical northwestern Pacific Ocean and the associated development of negative wind stress curl anomalies north of the equator since the EH, when the Walker Circulation was enhanced, may have favored an intensification of the northward NPG (including its western boundary current) (Figs. 1 and 6). Moreover, a strengthened western boundary current would have carried more heat to higher latitudes and also have intensified the extratropical westerlies (Gu and Philander, 1997). This would have subsequently resulted in more negative wind stress curl and a speed-up of the NPG.

Meanwhile, seasonal variations of the East Asian monsoon may also have affected the northward transport of the KC through speed-up/down of the NPG. The East Asian monsoon was also

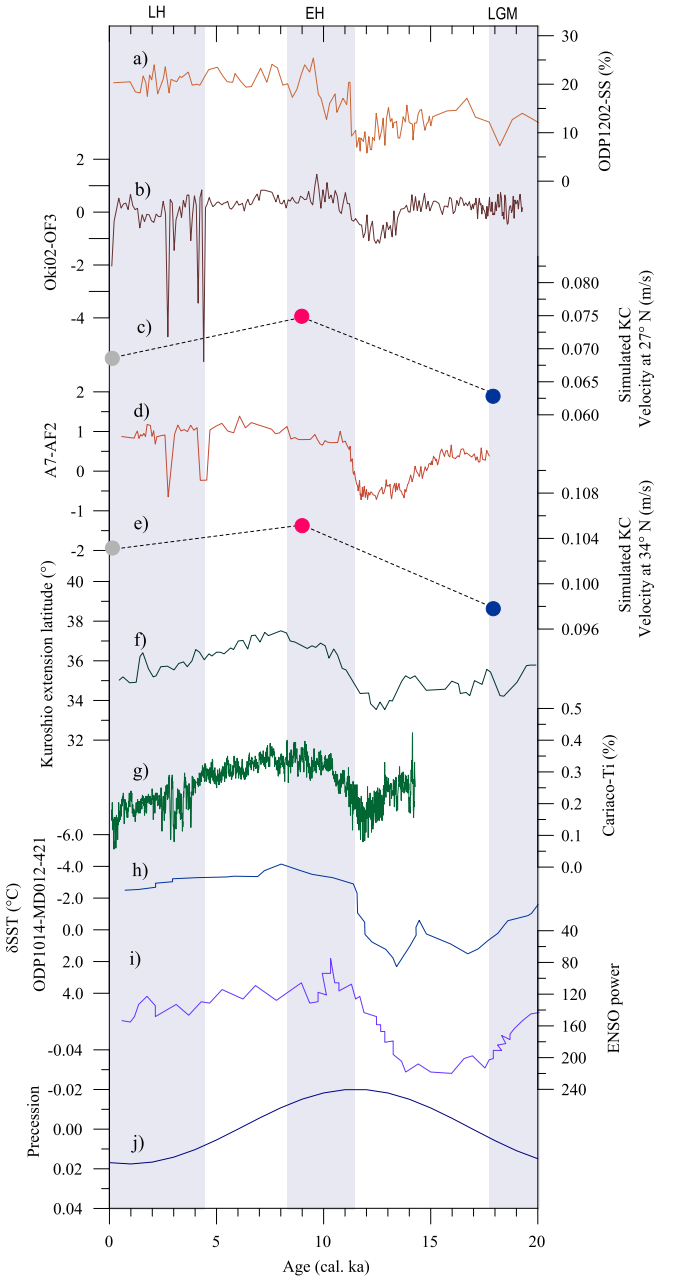

Fig. 9. a) Temporal variations of the percentage of the sortable silt (SS) fraction of core ODP1202 (Diekmann et al., 2008). b) The factor score of the KC index for AF2. c) KC strength at 27°N, as simulated in the COSMOS Model for LH, EH, and LGM. d) The factor score of the KC index for OF3. e) KC strength at 34°N, as simulated in the COSMOS Model for LH, EH, and LGM. f) Latitudinal variation of the Kuroshio extension, as revealed by the SST contrast between core St.19 and MD01-2421 (Yamamoto, 2009). g) ITCZ index, as indicated by Ti counts in the Cariaco Basin (Haug et al., 2001). h) North Pacific High (NP High) or ENSO indicator, as indicated by the SST contrast between core MD01-2421 and ODP1014 (Yamamoto et al., 2004). i) ENSO variability, as estimated from application of Zebiak–Cane-coupled ocean–atmosphere model forced by changing orbital parameters (Tudhope et al., 2001). j) The precessional cycle of orbital forcing (Berger and Loutre, 1991).

shown to be linked to the precessional variability of the Earth's perihelion via the north–south migration of the Intertropical Convergence Zone (Schneider et al., 2014). Since the EH, when the summer insolation in the North Hemisphere attained its maximum due to precessional forcing, the East Asian summer monsoon has intensified significantly in response to the northward migration of the Intertropical Convergence Zone (Haug et al., 2001; Schneider et al., 2014) (Fig. 9). In contrast, the East Asian win-

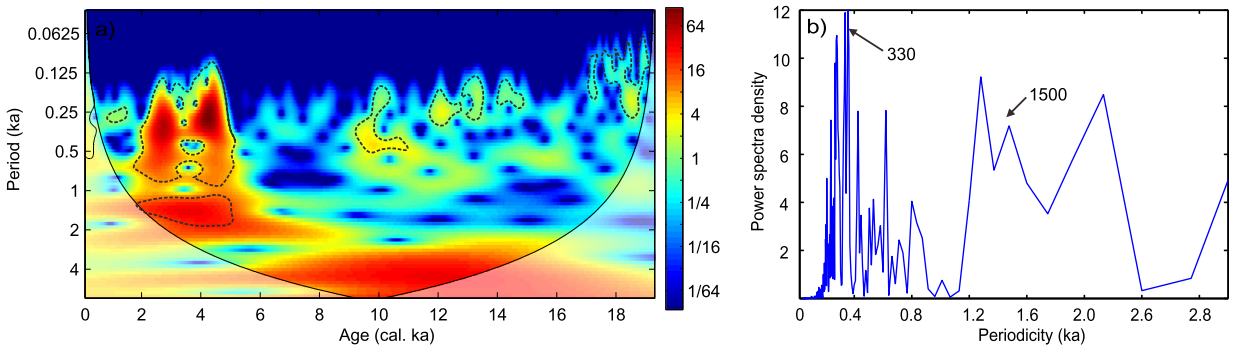

Fig. 10. a) Wavelet power spectrum on KC indicator OF3 with Morlet wavelet; dashed lines represent the 90% confidence level. b) Spectrum analyses for OF3.

ter monsoon was considerably weakened (Zheng et al., 2014). The strengthening of the southwest summer monsoon and weakening of the northeastern winter monsoon indicate more negative wind stress curl over the subtropical North Pacific, supporting strengthened NPG and KC. The corresponding speed-up westerlies would further enhance the NPG as positive feedback. In the Luzon Strait and the Okinawa Trough, these changes in the East Asian monsoon may also have favored a large poleward water transport in KC, but a reduced amount into the South China Sea (Qu et al., 2004). Our modeling experiments also supported an intensification in KC during the EH compared with LGM conditions.

On the other hand, the western branch of the NPG system, including the KC and the Kuroshio extension, changed synchronously with the long-term insolation-paced variability of ENSO since the LGM (Fig. 9). The general trend of the grain-size end member (AF2/OF3), characterizing the KC contribution to the grain-size spectrum, corresponded to the ΔSST_{NWP} between cores St.19 and MD01-2421 and the ΔSST_{NPH} between cores ODP1014 and MD01-2421 (Fig. 9). The high AF2 and OF3 values in the Okinawa Trough corresponded to the high ΔSST_{NWP} at the Japanese margin, indicating stronger and northward migration of the KC. Moreover, an ENSO-like variability pattern has been proposed as the primary driver of the mid-latitude North Pacific East–West SST seesaw on annual, decadal, and orbital scales (Yamamoto et al., 2004). The ΔSST_{NPH}, representing the SST contrast between the eastern and western mid-latitude Pacific, recorded the long-term variability of the North Pacific High and ENSO variability (Yamamoto et al., 2004). Modern observations during La Niña revealed that the tropical convection moves to the western equatorial Pacific as the East–West Equatorial Pacific sea surface temperature contrast is high and the easterly wind prevails, and vice versa during El Niño (Fig. 1). In other words, the higher the east–west SST gradient, westward warm-pool displacement, and acceleration of the trade winds during La Niña, the greater the negative wind stress curl in the Pacific Ocean (Hu et al., 2015). Moreover, these conditions are also indicative of an expansion in the subtropical gyre and shrinking of the tropical gyre (England et al., 2014; Hu et al., 2015). Model results also identified an expansion of the subtropical gyre during the EH and LH compared to the LGM (Figs. 1 and 6). All of these features will accelerate the NPG and the KC during La Niñas.

High frequency oscillations in the AF2/OF3 since 5 ka are consistent with the large century-scale variations in precipitation based on amplitudes of Ti content in the Cariaco Basin that have been interpreted as higher centennial-scale ENSO-like condition intervals (Haug et al., 2001) (Fig. 9). The equatorial oceans received more insolation during this period when the precession driven perihelion occurred during the boreal winter, which contributed to the larger event amplitudes (Clement et al., 2000). Storm sediments in an alpine lake revealed that modern ENSO periodicities were established after 5 ka, with the highest El Niño frequencies at 3.5∼2.6 ka (Rodbell et al., 1999). Modeling work indicated that ENSO was enhanced after 5 ka (Clement et al., 2000). Consistently, the East Asian winter monsoon and East Asian summer monsoon have exhibited high-amplitude variations since around 5 ka, as revealed by stalagmite and marine sediment records (Dykoski et al., 2005; Zheng et al., 2014). Therefore, the coupled high frequency ENSO and monsoon effects superimposed on the long-term trend may have changed the strength of the NPG via modulating the basin-wide wind stress curl, and thus the northward KC. Collectively, the data and model evidence indicated coherent and synchronous changes of the western branch of the NPG in response to insolation variability since the LGM.

5.5. Millennial-scale changes of the KC and the climate system

Wavelet analyses of OF3 variability revealed two dominant periodicities of approximately 1500 and 330 yrs during 5∼2 ka (Fig. 10). The 1500-yr cycle of the last 5∼2 ka is in line with the previously proposed KC cycle (Jian et al., 2000), and is also consistent with the millennial fluctuations of ENSO variability during the Holocene epoch (Moy et al., 2002). As suggested by Stott et al. (2002), the millennial-scale variations in the North Atlantic and tropical Pacific were controlled by ocean/atmospheric interactions, acting in the mode analogous to modern "super-ENSO". The Zebiak-Cane coupled ocean-atmosphere model has indicated that, under orbital configurations, ENSO may abruptly lock to the seasonal cycle and produce a mean sea surface temperature change in the tropical Pacific (Clement et al., 2001). Moreover, this change may have had a global impact and triggered millennial-scale climate changes (Clement et al., 2001). El Niño conditions correlated with stadials at high latitudes, whereas La Niña conditions correlated with interstadials (Stott et al., 2002). As discussed above, during the El Niño-like state, the tropical gyre was strengthened and the NPG was weakened, as more heat was stored in the tropics and less was transported northward through a western boundary current, such as the KC. Increased Pacific sea surface temperature during the El Niño-like state led to a larger latitudinal temperature gradient, transporting more moisture to high latitudes through greater Hadley cell intensity and stronger eddy transport, and ultimately creating a surge in ice (Turney et al., 2004). These changes also influenced North Atlantic deep water formation, which has been linked with less heat being transported northward by the subtropical gyres.

The significance of this cycle (1500 yrs) is also the subject of an on-going debate regarding its precise dates and forcing mechanisms (Isono et al., 2009; Sorrel et al., 2012). The main issue of this controversy is related to its reproducibility during the Holocene (Isono et al., 2009). The occurrence of this cycle throughout both the Holocene and the last glacial period may support a precise millennial clock. However, the findings of the 1500-yr cycle of Holocene storm dynamics in the North Atlantic Ocean

(Sorrel et al., 2012) support internal noise as the main driver. Bond et al. (2001) proposed that a solar forcing mechanism underlied at least the Holocene segment of the North Atlantic "1500-yr" cycle. The surface hydrographic changes potentially acted as an additional mechanism for amplifying the solar signals and transmitting them globally (Bond et al., 2001). The findings of the millennial scale changes in KC strength during the Holocene supported a precise dating mechanism. The millennial signal in KC could be transmitted northward by NPG, and thus influenced the North Atlantic regions via the Westerlies. Overall, the millennial oscillation of the KC during the Holocene interval might provide stronger support for the hypothesis that this periodicity constitutes a precise "heartbeat" of the Earth's climate.

6. Conclusion

As the Northern Pacific western boundary current, the KC plays a critical role in regulating heat and moisture transport in the Northeast Asian region. Based on grain-size spectra, clay mineral, and Sr–Nd isotope constraints of sediments from the northern Okinawa Trough, we reconstructed changes in KC dynamics over the past 20 ka. Combined with published sediment records surrounding the NPG and Earth-System-Model simulations, we showed that the KC remained in the Okinawa Trough throughout the LGM interval and intensified greatly since the EH which shaped the sediment transport configuration. This then altered the sediment flux and clay mineral provenance when a large shelf area was submerged during a period of high sea level. The change in KC is possibly related to the precession- induced increase in the occurrence of La Niña-like state and the strength of the East Asian monsoon. The coherent and concurrent shift of the KC and Kuroshio extension with the changing ENSO variability may further indicate that the western branch of the NPG is ultimately subject to a basin-wide change in wind stress curl in the Pacific in response to precession forced change in insolation. On the other hand, large century-scale variations in the KC occurring since 5 ka ago, especially during the *Pulleniatina* Minimum Event, are attributable to the establishment of the modern ENSO conditions superimposed on the longer-term trend when the equatorial oceans experienced stronger insolation during the boreal winter.

Acknowledgements

Our work is supported by the National Natural Science Foundation of China (41506051, 91128206, 41376057, 91328207, and 41430965), the Strategic Priority Research Program of the Chinese Academy of Sciences (XDA11030302), the Guangdong Natural Science Foundation (KLMMR-2015-B-07) and the Key Laboratory of Marginal Sea Geology, Chinese Academy of Sciences (MSGL15-10). We thank Prof. Heather Stoll, Prof. Gerrit Lohmann, Prof. Amy Clement, Prof. Zhonghui Liu and four anonymous reviewers for their help and suggestions on this manuscript.

Appendix A. Supplementary material

Supplementary material related to this article can be found online at http://dx.doi.org/10.1016/j.epsl.2016.07.028.

References

Andres, M., Jan, S., Sanford, T.B., Mensah, V., Centurioni, L.R., Book, J.W., 2015. Mean structure and variability of the Kuroshio from northeastern Taiwan to southwestern Japan. Oceanography 28, 84–95.

Berger, A., Loutre, M.-F., 1991. Insolation values for the climate of the last 10 million years. Quat. Sci. Rev. 10, 297–317.

Bond, G., Kromer, B., Beer, J., Muscheler, R., Evans, M.N., Showers, W., Hoffmann, S., Lotti-Bond, R., Hajdas, I., Bonani, G., 2001. Persistent solar influence on North Atlantic climate during the Holocene. Science 294, 2130–2136.

Chen, H.-F., Chang, Y.-P., Kao, S.-J., Chen, M.-T., Song, S.-R., Kuo, L.-W., Wen, S.-Y., Yang, T.-N., Lee, T.-Q., 2011. Mineralogical and geochemical investigations of sediment-source region changes in the Okinawa trough during the past 100 ka (IMAGES core MD012404). J. Asian Earth Sci. 40, 1238–1249.

Clement, A., Seager, R., Cane, M., 1999. Orbital controls on the El Nino/Southern Oscillation and the tropical climate. Paleoceanography 14, 441–456.

Clement, A.C., Seager, R., Cane, M.A., 2000. Suppression of El Niño during the Mid-Holocene by changes in the Earth's orbit. Paleoceanography 15, 731–737.

Clement, A.C., Cane, M.A., Seager, R., 2001. An orbitally driven tropical source for abrupt climate change. J. Climate 14, 2369–2375.

Diekmann, B., Hofmann, J., Henrich, R., Fütterer, D.K., Röhl, U., Wei, K.-Y., 2008. Detrital sediment supply in the southern Okinawa trough and its relation to sea-level and Kuroshio dynamics during the late quaternary. Mar. Geol. 255, 83–95.

Dou, Y., Yang, S., Liu, Z., Clift, P.D., Yu, H., Berne, S., Shi, X., 2010. Clay mineral evolution in the central Okinawa trough since 28 ka: implications for sediment provenance and paleoenvironmental change. Palaeogeogr. Palaeoclimatol. Palaeoecol. 288, 108–117.

Dou, Y., Yang, S., Liu, Z., Shi, X., Li, J., Yu, H., Berne, S., 2012. Sr–Nd isotopic constraints on terrigenous sediment provenances and Kuroshio Current variability in the Okinawa Trough during the late Quaternary. Palaeogeogr. Palaeoclimatol. Palaeoecol. 365, 38–47.

Dykoski, C.A., Edwards, R.L., Cheng, H., Yuan, D., Cai, Y., Zhang, M., Lin, Y., Qing, J., An, Z., Revenaugh, J., 2005. A high-resolution, absolute-dated Holocene and deglacial Asian monsoon record from Dongge Cave, China. Earth Planet. Sci. Lett. 233, 71–86.

England, M.H., McGregor, S., Spence, P., Meehl, G.A., Timmermann, A., Cai, W., Gupta, A.S., McPhaden, M.J., Purich, A., Santoso, A., 2014. Recent intensification of wind-driven circulation in the Pacific and the ongoing warming hiatus. Nature Climate Change 4, 222–227.

Gong, X., Zhang, X., Lohmann, G., Wei, W., Zhang, X., Pfeiffer, M., 2015. Higher Laurentide and Greenland ice sheets strengthen the North Atlantic ocean circulation. Clim. Dyn. 45, 139–150.

Gu, D., Philander, S.G., 1997. Interdecadal climate fluctuations that depend on exchanges between the tropics and extratropics. Science 275, 805–807.

Guo, X., Zhu, X.H., Wu, Q.S., Huang, D., 2012. The Kuroshio nutrient stream and its temporal variation in the East China Sea. J. Geophys. Res., Oceans (1978–2012) 117, C01026. http://dx.doi.org/10.1029/2011JC007292.

Haug, G.H., Hughen, K.A., Sigman, D.M., Peterson, L.C., Rohl, U., 2001. Southward migration of the intertropical convergence zone through the Holocene. Science 293, 1304–1308.

Hu, D., Wu, L., Cai, W., Gupta, A.S., Ganachaud, A., Qiu, B., Gordon, A.L., Lin, X., Chen, Z., Hu, S., 2015. Pacific western boundary currents and their roles in climate. Nature 522, 299–308.

Isono, D., Yamamoto, M., Irino, T., Oba, T., Murayama, M., Nakamura, T., Kawahata, H., 2009. The 1500-year climate oscillation in the midlatitude North Pacific during the Holocene. Geology 37, 591–594.

Jian, Z., Wang, P., Saito, Y., Wang, J., Pflaumann, U., Oba, T., Cheng, X., 2000. Holocene variability of the Kuroshio Current in the Okinawa trough northwestern Pacific Ocean. Earth Planet. Sci. Lett. 184, 305–319.

Jiang, F., Frank, M., Li, T., Chen, T.Y., Xu, Z., Li, A., 2013. Asian dust input in the western Philippine Sea: evidence from radiogenic Sr and Nd isotopes. Geochem. Geophys. Geosyst. 14, 1538–1551.

Kao, S., Horng, C., Hsu, S., Wei, K., Chen, J., Lin, Y., 2005. Enhanced deepwater circulation and shift of sedimentary organic matter oxidation pathway in the Okinawa trough since the Holocene. Geophys. Res. Lett. 32, L15609. http://dx.doi.org/10.1029/2005GL023139.

Lee, H.-J., Chao, S.-Y., 2003. A climatological description of circulation in and around the East China Sea. Deep-Sea Res., Part 2, Top. Stud. Oceanogr. 50, 1065–1084.

Li, T., Xu, Z., Lim, D., Chang, F., Wan, S., Jung, H., Choi, J., 2015. Sr–Nd isotopic constraints on detrital sediment provenance and paleoenvironmental change in the northern Okinawa trough during the late quaternary. Palaeogeogr. Palaeoclimatol. Palaeoecol. 430, 74–84.

Lin, Y.-S., Wei, K.-Y., Lin, I.-T., Yu, P.-S., Chiang, H.-W., Chen, C.-Y., Shen, C.-C., Mii, H.-S., Chen, Y.-G., 2006. The Holocene Pulleniatina minimum event revisited: geochemical and faunal evidence from the Okinawa trough and upper reaches of the Kuroshio current. Mar. Micropaleontol. 59, 153–170.

Liu, J.P., Milliman, J.D., Gao, S., Cheng, P., 2004. Holocene development of the Yellow River's subaqueous delta, North Yellow Sea. Mar. Geol. 209, 45–67.

Luo, C., Zheng, H., Wu, W., Wang, P., Chen, Y., Wei, X., 2012. Sr–Nd isotope stratification along water depth: an example from Datong hydrological station of Yangtze River. Chin. Sci. Bull. 57, 4482–4490.

Moy, C.M., Seltzer, G.O., Rodbell, D.T., Anderson, D.M., 2002. Variability of El Niño/southern oscillation activity at millennial timescales during the Holocene epoch. Nature 420, 162–165.

Oguri, K., Matsumoto, E., Saito, Y., Honda, M.C., Harada, N., Kusakabe, M., 2000. Evidence for the offshore transport of terrestrial organic matter due to the rise of sea level: the case of the East China Sea continental shelf. Geophys. Res. Lett. 27, 3893–3896.

Qu, T., Kim, Y.Y., Yaremchuk, M., Tozuka, T., Ishida, A., Yamagata, T., 2004. Can luzon strait transport play a role in conveying the impact of ENSO to the South China Sea? J. Climate 17, 3644–3657.

Rodbell, D.T., Seltzer, G.O., Anderson, D.M., Abbott, M.B., Enfield, D.B., Newman, J.H., 1999. An ~15,000-year record of El Niño-driven alluviation in southwestern Ecuador. Science 283, 516–520.

Schneider, T., Bischoff, T., Haug, G.H., 2014. Migrations and dynamics of the intertropical convergence zone. Nature 513, 45–53.

Smith, V.C., Staff, R.A., Blockley, S.P., Ramsey, C.B., Nakagawa, T., Mark, D.F., Takemura, K., Danhara, T., 2013. Identification and correlation of visible tephras in the Lake Suigetsu SG06 sedimentary archive, Japan: chronostratigraphic markers for synchronising of east Asian/west Pacific palaeoclimatic records across the last 150 ka. Quat. Sci. Rev. 67, 121–137.

Sorrel, P., Debret, M., Billeaud, I., Jaccard, S.L., McManus, J.F., Tessier, B., 2012. Persistent non-solar forcing of Holocene storm dynamics in coastal sedimentary archives. Nat. Geosci. 5, 892–896.

Stommel, H., 1948. The westward intensification of wind-driven ocean currents. Eos, Trans. Am. Geophys. Union 29, 202–206.

Stott, L., Poulsen, C., Lund, S., Thunell, R., 2002. Super ENSO and global climate oscillations at millennial time scales. Science 297, 222–226.

Sun, Y., Oppo, D.W., Xiang, R., Liu, W., Gao, S., 2005. Last deglaciation in the Okinawa trough: subtropical northwest Pacific link to Northern Hemisphere and tropical climate. Paleoceanography 20, PA4005. http://dx.doi.org/10.1029/2004PA001061.

Sverdrup, H.U., 1947. Wind-driven currents in a baroclinic ocean; with application to the equatorial currents of the eastern Pacific. Proc. Natl. Acad. Sci. USA 33, 318.

Tudhope, A.W., Chilcott, C.P., McCulloch, M.T., Cook, E.R., Chappell, J., Ellam, R.M., Lea, D.W., Lough, J.M., Shimmield, G.B., 2001. Variability in the El Niño–Southern Oscillation through a glacial–interglacial cycle. Science 291, 1511–1517.

Turney, C.S., Kershaw, A.P., Clemens, S.C., Branch, N., Moss, P.T., Fifield, L.K., 2004. Millennial and orbital variations of El Nino/Southern Oscillation and high-latitude climate in the last glacial period. Nature 428, 306–310.

Ujiié, H., Hatakeyama, Y., Gu, X.X., Yamamoto, S., Ishiwatari, R., Maeda, L., 2001. Upward decrease of organic C/N ratios in the Okinawa trough cores: proxy for tracing the post-glacial retreat of the continental shore line. Palaeogeogr. Palaeoclimatol. Palaeoecol. 165, 129–140.

Wang, J., Li, A., Xu, K., Zheng, X., Huang, J., 2015. Clay mineral and grain size studies of sediment provenances and paleoenvironment evolution in the middle Okinawa trough since 17 ka. Mar. Geol. 366, 49–61.

Wei, W., Lohmann, G., 2012. Simulated Atlantic multidecadal oscillation during the Holocene. J. Climate 25, 6989–7002.

Weltje, G.J., Prins, M.A., 2003. Muddled or mixed? Inferring palaeoclimate from size distributions of deep-sea clastics. Sediment. Geol. 162, 39–62.

Xiang, R., Sun, Y., Li, T., Oppo, D.W., Chen, M., Zheng, F., 2007. Paleoenvironmental change in the middle Okinawa trough since the last deglaciation: evidence from the sedimentation rate and planktonic foraminiferal record. Palaeogeogr. Palaeoclimatol. Palaeoecol. 243, 378–393.

Yamamoto, M., Oba, T., Shimamune, J., Ueshima, T., 2004. Orbital-scale anti-phase variation of sea surface temperature in mid-latitude North Pacific margins during the last 145,000 years. Geophys. Res. Lett. 31, L16311. http://dx.doi.org/10.1029/2004GL020138.

Yamamoto, M., 2009. Response of mid-latitude North Pacific surface temperatures to orbital forcing and linkage to the East Asian summer monsoon and tropical ocean–atmosphere interactions. J. Quat. Sci. 24, 836–847.

Yang, Z., Guo, Z., Wang, Z., Xu, J., Gao, W., 1992. Basic pattern of transport of suspended matter from the Yellow Sea and East China Sea to the eastern deep seas. Acta Oceanol. Sin. 14, 81–90.

Zheng, X., Li, A., Wan, S., Jiang, F., Kao, S.J., Johnson, C., 2014. ITCZ and ENSO pacing on East Asian winter monsoon variation during the Holocene: sedimentological evidence from the Okinawa trough. J. Geophys. Res., Oceans 119, 4410–4429.

Zheng, X., Li, A., Wan, S., Jiang, F., Yin, X., Lu, J., 2015. Formation of the modern current system in the East China Sea since the early Holocene and its relationship with sea level and the monsoon system. Chin. J. Oceanol. Limnol. 33, 1062–1071.

Zheng, Z., Yang, S., Deng, Y., Huang, K., Wei, J., Berne, S., Suc, J.-P., 2011. Pollen record of the past 60 ka BP in the middle Okinawa trough: terrestrial provenance and reconstruction of the paleoenvironment. Palaeogeogr. Palaeoclimatol. Palaeoecol. 307, 285–300.